Thin Solid Films 763 (2022) 139578

Contents lists available at ScienceDirect

Thin Solid Films

journal homepage: www.elsevier.com/locate/tsf

Approach to quantitative detection of proteins with the biosensor based on imaging ellipsometry and spectroscopic ellipsometry

Chenyu Wang [a,b,c], Wei Liu [a,b,*], Yu Niu [a,b], Peng Xu [a,b], Gang Jin [d]

[a] NML, Institute of Mechanics, Chinese Academy of Sciences, 15 Bei-si-huan West Road, Beijing 100190, China
[b] Center for Gravitational Wave Experiment, Institute of Mechanics, Chinese Academy of Sciences, 15 Bei-si-huan West Road, Beijing 100190, China
[c] School of Engineering Science, University of Chinese Academy of Sciences, 19 Yu-quan Road, Beijing 100049, China
[d] School of Foundamenal Physics and Mathematical Sciences, Hangzhou Institute for Advanced Study, University of Chinese Academy of Sciences, Hangzhou 310024, China

ARTICLE INFO

Keywords:
Imaging ellipsometry
Biosensor
Quantitative detection

ABSTRACT

The biosensor based on imaging ellipsometry (BIE) is a practical technique to measure protein interactions such as the immobilization of biomolecules and the recognition between ligand and analyte. In this paper, to avoid the working condition optimization before each measurement, a fixed linear working condition for the silicon wafer chip is established at the angle of incidence of 75° with the fixed azimuths of the polarizer and the analyzer $P = 90°$ and $A = 45°$. Further, a quantitative model is constructed to establish the standard curve between the ellipsometric signal and the protein concentration. As a result, this model is used to deduce the dissociation equilibrium constants of three relevant blood proteins as well as their antibodies. This work bridges the gap between the biochemical demand and BIE for sensing applications.

1. Introduction

A biosensor based on imaging ellipsometry (BIE), as a label-free, high sensitivity characterization technique for a thin layer [1,2], has greatly progressed since the concept put forward in 1995 [3]. It is a direct optical visualization method that offers a distinct graph for qualitative or quantitative analysis of protein interactions on a solid surface. Compared with the traditional immunoassays for proteins measurement such as enzyme linked immunosorbent assay (ELISA) [4], a label-free method offers advantages as a direct means of detecting protein-protein binding and avoids the limitations of labeling. For example, labeling may affect the activity of the binding site on small molecules, or face the need for excitation and fluorescent bleaching in fluorescence tags. To date, various non-labeling detection methods have been reported including surface plasmon resonance (SPR), atomic force microscopy (AFM) and quartz crystal microbalance (QCM), etc.. Although SPR technique can meet the requirement of high throughput, the sensitivity is limited [5]. AFM with high lateral resolution is destructive to the sample and requires specific working condition [6]. QCM is often operated in dry air or nitrogen in order to guarantee the identical conditions before and after each measurement of the process [7]. Thus, BIE with advantages of label-free, non-destruction, good sensitivity and simplicity can be used as a powerful method for protein detection. It has already been applied to monitoring antigen-antibody kinetics [8,9], disease biomarkers detection [10,11] and environmental pollution monitoring [12].

However, the azimuths of the polarizer and the analyzer need to be optimized to get a sensitive response to the protein binding interaction before each measurement in application, which limits the promotion and use of the sensor. For sensor applications, the users prefer focusing on the sample measurement to the optimization of the equipment. Thus, the azimuths of the polarizer and the analyzer should be fixed. Further, in biochemical applications, instead of the ellipsometric parameters such as ψ and Δ or the thickness of the layer, a standard curve on the signal vs. sample concentration is preferable. It is worthy of constructing a detailed quantitative model which could bridge the gap between the biochemical demand and BIE.

In this paper, we optimize the azimuths of the polarizer and the analyzer for our sensing purpose. Since spectroscopic ellipsometry (SE) can tell about 0.1 nm film thickness variation which is widely used to measure the film properties by collecting the amplitude ratio and phase difference of the reflected polarized light [13], a quantitative model is constructed to establish the correlation between the ellipsometric signal and protein concentration. Furthermore, three relevant blood proteins

* Corresponding author.
E-mail address: liuwei@imech.ac.cn (W. Liu).

https://doi.org/10.1016/j.tsf.2022.139578
Received 31 August 2022; Received in revised form 2 November 2022; Accepted 2 November 2022
Available online 4 November 2022

as well as their antibodies are used to testify the model.

2. Experimental details

2.1. Chemicals and materials

The silicon substrate has a silica layer of approximately 2 nm, P-type monocrystalline silicon doped with boron, purchased from the General Research Institute for Nonferrous Metals (China). Components of the study including 3-aminopropyltriethoxy-silane (APTES), glutaraldehyde (Glu), human immunoglobulin G (IgG), goat anti-IgG, bovine serum albumin (BSA), rabbit anti-BSA, human fibrinogen (Fib) and goat anti-Fib are produced by Sigma-Aldrich (Missouri, USA) and used without further purification. All solutions are prepared in ultrapure water produced by a Millipore Milli-Q ion exchange apparatus. The proteins are diluted to different concentrations by using phosphate buffered saline (PBS) (pH 7.4 at 25 °C).

2.2. Ellipsometry measurement system

The experiments are carried out with the BIE developed in our laboratory and the SE (J. A, Woollam RC2) respectively. BIE system consists of microfluidic array system used for surface patterning and array fabrication as well as imaging ellipsometry (IE) used for reading the protein adsorption layer [14]. As a typical ellipsometry technique, IE is based on a polarizer-compensator-sample-analyze (PCSA) configuration shown in Fig. 1(a). The Xenon lamp light beam is directed to a collimating and extending system after passing through an optical filter at 632.8 nm wavelength which increase the ellipsometric contrast of image. The linearly polarized light beam strikes the sample at the angle of incidence of 75° after passing via a compensator (quarter wave plate) after the polarizer. Following the reflection, the light beam passes through a second polarizer, which is termed as the analyzer, and is received into the charge coupled device (CCD). The signal of IE is the light reflection intensity of the fabricated protein microarray surface which could describe the adsorption of the protein layer intuitively. The distribution of the protein layer thickness is simultaneously detected by SE. In our current work, the RC 2-D of J. A Woollam with a spectrum of 193–1000 nm is applied to examine various protein samples at the angle of incidence 75 °. For saturated and dense single-layer protein film, the six layers structure model (Air - Cauchy layer - Self assembled monolayers (SAMs) - SiO_2 - Interface layer - Si substrate) is used to fit the thickness of protein film in order to approximate the actual physical configuration, and the thickness measurement precision can reach 0.1 nm. (The refractive index for proteins absorbed on the Si substrate are in the range of 1.48–1.57 according to previous work [15], and for the fitting process of the same protein sample, the refractive index is regarded as invariant.)

2.3. Procedures

Take the IgG/anti-IgG as an example. The general detection procedure for the protein adsorption layer is depicted in Fig. 1(b) including surface modification, ligand immobilization, and analyte binding. Referencing our previous stuff [16], the surface modification procedure of silicon wafers as the IE immunosensor substrates is modified with SAMs by coupling APTES and Glu. To prepare the ligand immobilization, IgG solutions of various concentrations (0.006, 0.06, 0.3, 0.6, 3, 6, 30 and 80 μg ml^{-1}) enter the surface through the microarray at 1 μL min^{-1} for 10 min followed by washing with PBS. The unit with saturated ligand molecular layer with enough high concentration (80 μg ml^{-1}) of IgG solution will continue the binding process of analyte. Previously, the blocking buffer is injected at 1 μL min^{-1} for 30 min to block the non-specific binding sites with the subsequent washing with PBS. Then

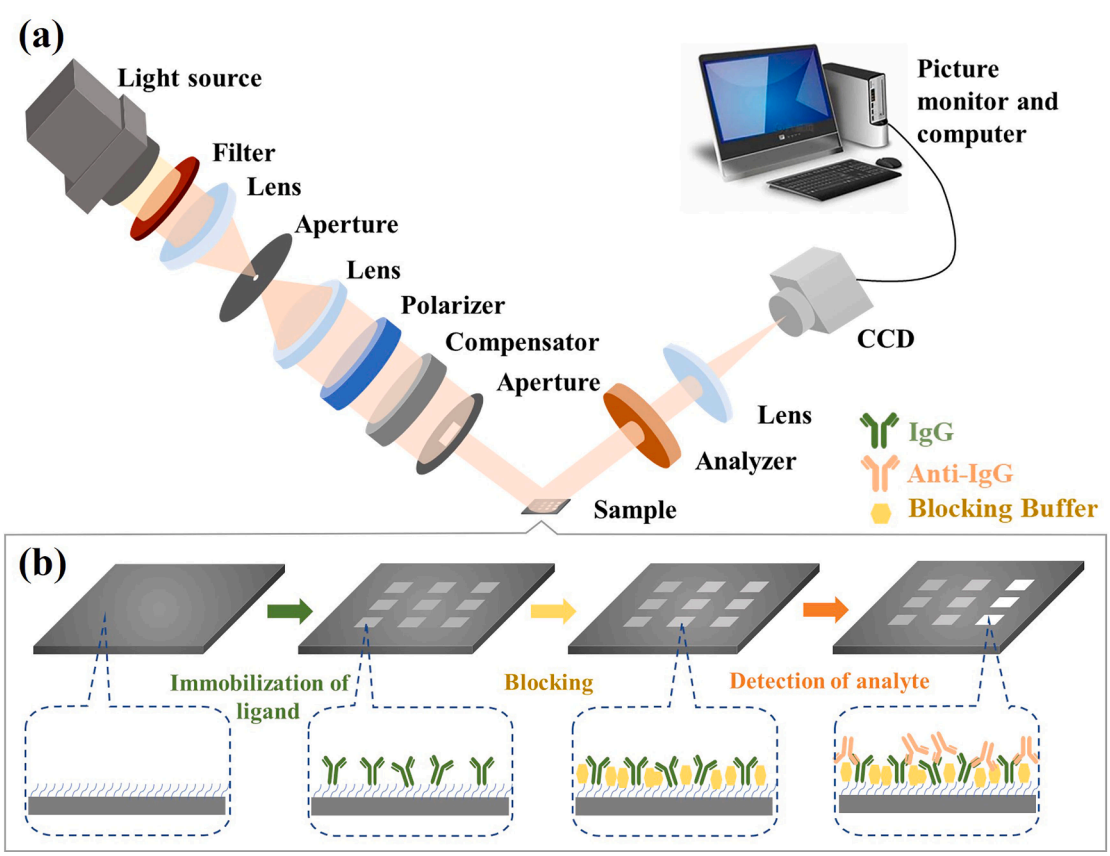

Fig. 1. (a) Schematic diagram of BIE based on PCSA configuration; (b) Schematic diagram of ligand immobilization and analyte recognition on the protein microarray.

the anti-IgG solutions with the same concentrations ratio as the ligand solutions are injected to react with saturated IgG specifically at 1 μL min^{-1} for 10 min. After being rinsed and dried, the surface information of surface-bound protein is measured by IE and SE, respectively.

Considering the current procedure, ligand molecules (IgG) can covalently bind to different areas of the modified substrate due to the Schiff reaction between aldehyde group (-CHO) on the surface and amino group (-NH2) in the ligand protein. In this case, each IgG bound area of the microarray may function as a probe which can capture the corresponding target (anti-IgG) in the analyte solution. When the anti-IgG in the solution interact with the probe in the microarray, they form a complex due to the affinity and the layer covering the surface area of the interaction becomes thick (or surface grayscale increase). A significant increase in the attached layer thickness (or surface grayscale) indicates that the solution contains the analyte anti-IgG.

3. Theory

3.1. The optimal azimuths of the polarizer and the analyzer for linear off-null working condition of BIE

We need to fix the optimal azimuths of the polarizer and the analyzer for BIE biochemical applications. In general, the expression for the detected intensity of IE in a typical PCSA system is given by [17]

$$I = G\frac{|R_s|^2}{4\cos^2\psi}[1-\cos2\psi\cos2A+\sin2\psi\sin(2P+\Delta)\sin2A] \tag{1}$$

where ψ and Δ are the ellipsometric parameters defined by $\tan\psi = |R_p|/|R_s|$ and $\Delta = \Delta_p - \Delta_s$ when $R_p = |R_p|exp(j\Delta_p)$ and $R_s = |R_s|exp(j\Delta_s)$ are the complex reflection coefficients for p and s polarized parts, respectively. P and A are the azimuths of polarizer and analyzer. G is a device dependent parameter.

For the sensing applications, our imaging ellipsometry biosensor often focuses on the relative change at the interface instead of the exact ellipsometric parameters, which implies the maximum detected intensity variation after the adsorption at the optimal azimuths of the polarizer and the analyzer. Further, a linear response is expected for the small variations. Thus, the Taylor expansion of Eq. (1) is given by

$$\delta I = G\frac{|R_s|^2}{2\cos^2\psi}[\tan\psi+\cos2A\tan\psi+\sin2A\sin(2P+\Delta)]\delta\psi + G\frac{|R_s|^2}{4\cos^2\psi}\sin2A\sin2\psi\cos(2P+\Delta)\delta\Delta \tag{2}$$

Let's denote $f = \delta I$, thus, to optimize the azimuths of P, we have $\frac{\partial f}{\partial P} = 0$, that is

$$G\frac{|R_s|^2}{\cos^2\psi}\sin2A\cos(2P+\Delta)\delta\psi - G\frac{|R_s|^2}{2\cos^2\psi}\sin2A\sin2\psi\sin(2P+\Delta)\delta\Delta = 0 \tag{3a}$$

Or

$$\tan(2P+\Delta) = \frac{2}{\sin2\psi}\frac{\delta\psi}{\delta\Delta} \tag{3b}$$

When $\delta\psi \ll \delta\Delta$ $\tan(2P+\Delta) \approx 0$, $P = -\frac{\Delta}{2}$ or $P = \frac{\pi}{2} - \frac{\Delta}{2}$

In our BIE configuration, silicon wafer is used as the substrate, in the neighborhood around pseudo-Brewster angle of which Δ jumps from -180° to 0°. For example, at the angle of incidence of 75°, $\Delta \approx 180^\circ$, $P = \pm 90^\circ$. For $\frac{\partial f}{\partial A} = 0$, we get

$$\frac{\partial f}{\partial A} = G\frac{|R_s|^2}{2\cos^2\psi}(-2\sin2A\tan\psi)\delta\psi + G\frac{|R_s|^2}{4\cos^2\psi}(2\cos2A\sin2\psi)\delta\Delta = 0 \tag{4a}$$

or

$$\cot2A = \frac{2\tan\psi}{\sin2\psi}\frac{\delta\psi}{\delta\Delta} \approx 0 \tag{4b}$$

Thus $A = \pm 45^\circ$ and the maximum detected intensity is

$$\delta I = G\frac{|R_s|^2}{2\cos^2\psi}\tan\psi\delta\psi + G\frac{|R_s|^2}{4\cos^2\psi}\sin2\psi\delta\Delta \tag{5}$$

Eq. (5) suggests a linear off-null working condition in which $I_0 \neq 0$, the detected signal varies linearly with the perturbation of the ellipsometric parameters which is advantageous for small signal variation compared with a quadratic variation of the conventional null-off null condition.

On the other hand, the ellipsometric parameters $\delta\psi$, $\delta\Delta$, is proportional to the layer thickness variation δd [18]

$$\delta\psi \propto \delta d, \delta\Delta \propto \delta d \tag{6}$$

According to Eqs. (5) and (6), we have

$$\delta I \propto \delta d \tag{7}$$

Therefore, it is not hard to obtain the variation connections between the detected light intensity and the layer thickness. Fig. 2(a) shows the ellipsometric parameter variation from the growth of 1 nm SiO_2 ($n = 1.457$) on the silicon substrate at the angles of incidence from 73° to 78° under the wavelength of 632.8 nm. It can be seen that the maximum amplitude change can be achieved at 75.5°, the pseudo-Brewster angle, and the phase difference jumps from -180° to 0° around the angle. Thus, the incident angle is set at 75°, near the pseudo-Brewster angle, to exploit the sensitivities from both ellipsometric parameters. As is seen in Fig. 2(b), two working conditions are compared when the thickness of SiO_2, d, disturbs less than 10 nm at the angle of incidence $\phi_0 = 75^\circ$. The response to the disturbance is parabolic under the traditional null-off null condition and the responses under the linear off-null condition are 10 times higher than that of the null-off null condition. Under the optimal azimuths of $P = 89.6^\circ$ and $A = 44.8^\circ$, the maximum response is almost the same as that of $P = 90^\circ$ and $A = 45^\circ$ (represented by red dashed and solid lines, respectively). Thus, the angle of incidence is set to 75° and the azimuths of the polarizer and the analyzer is fixed at $P = 90^\circ$ and $A = 45^\circ$ for the sensing application. There is a linear relationship between the detection light intensity and the film thickness.

3.2. The IE signal response to the protein concentration

Eq. (7) suggests that the increase of the film thickness of the protein layer δd is proportional to the light reflection intensity δI. However, it is of interest to obtain the surface mass density $\Gamma(\mu g/cm^2)$ rather than the layer thickness d (nm) for protein film measurement. The surface mass density is calculated by using de Feijter's equation [17].

$$\Gamma = \frac{d_f(n_f - n_a)}{dn/dc} \tag{8}$$

where n_f is the refractive index and d_f the thickness of the mixed polyelectrolyte multilayer. The dn/dc and n_f are assumed constant in this case and must be determined independently. The relation of the variations between the surface concentration and film thickness is given by

$$\delta\Gamma = \frac{(n_f - n_a)}{dn/dc}\delta d \tag{9}$$

Eqs. (7) and (9) in combination lead to

$$\delta I \propto \delta\Gamma = \delta\gamma \cdot M \tag{10}$$

where $\delta\gamma$ and M represent the amount of surface density of the protein layer and the protein molecular weight, respectively.

Equation (14) implies that for a given protein layer, the signal variation for IE is proportional to the amount of surface density of the

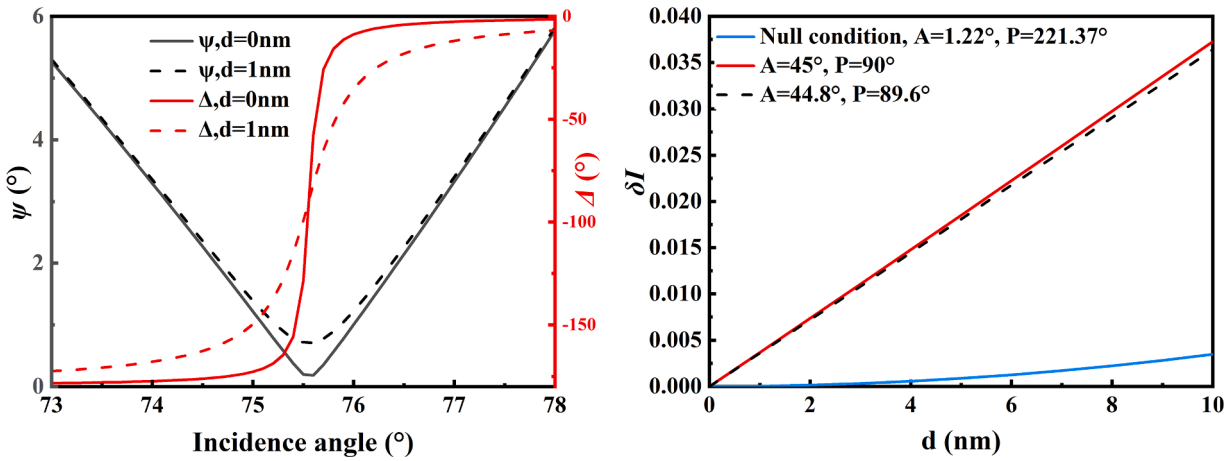

Fig. 2. (a) The ellipsometric parameter variation from the growth of 1 nm SiO_2 ($n = 1.457$) on the silicon substrate at the angles of incidence from 73° to 78°; (b) The signal responses to SiO_2 film less than 10 nm under null-off null condition (black line) and linear off null condition (red line).

protein film. Therefore, BIE combined IE and microarray in this work can monitor the biomolecules quantitatively.

As mentioned in 2.3, the modified surface formed by the SAMs can capture the ligand by the Schiff base reaction, achieving the covalent immobilization of the ligand, firstly. Then the ligand on the substrate interacts with the analyte in the solution to form ligand-analyte complex, enabling analyte recognition. Since the time-scale of the protein interactions is around the nano-second level, these reactions can be considered as quasi-equilibrium in our measurement time. Moreover, it is practicable and appropriate to approximate equilibrium with quasi-equilibrium in the short-term reaction time of few minutes as far as sensing is concerned because the time scale for complete equilibrium of proteins interaction might range from seconds to days. Thus, the ligand immobilization is regard as a dynamic equilibrium process performed by

$$Substrate - CHO + Protein - NH_2 \underset{k_d}{\overset{k_a}{\rightleftharpoons}} Substrate - CH = N - Protein$$

When S equals *Substrate-CHO, Ligand* equals Protein-NH_2, *S-Ligand* equals the complex. the reaction above can be expressed as

$$S + Ligand \underset{k_d}{\overset{k_a}{\rightleftharpoons}} S - Ligand$$

where k_a and k_d are the association rate constant and the dissociation rate constant, respectively, and thus the dissociation equilibrium constant $K_D = k_a/k_d$.

Under a pseudo-first-order interaction assumption, a link between the variation of surface mass density of the IE caused by the formation of the $S - Ligand$ complex and the ligand concentration in solution is derived [10]. According to the Eq. (10), the light reflection intensity can be further expressed by

$$\delta I_{Ligand} \propto \delta\Gamma_{Ligand} = \gamma_{S-Ligand} \cdot M_{Ligand} = \frac{(\gamma_s)_0 \cdot c_{Ligand}}{K_D + c_{Ligand}} \cdot M_{Ligand} \tag{11}$$

where c_{Ligand} are the concentrations of the ligand in solution, which can be regarded as a constant since the ligand solution is continuously and uniformly transported to the sensing surface through the microfluidic system. And $(\gamma_s)_0$ stands for the initial amount of the -CHO before ligand solution is delivered to the sensing substrate.

Similarly, the process of specific recognition of analytes and ligands can be formulated as

$$S - Ligand + Analyte \underset{k'_d}{\overset{k'_a}{\rightleftharpoons}} S - Ligand - Analyte$$

where k'_a and k'_d are the association rate constant and the dissociation rate constant of recognition, respectively, and thus the dissociation equilibrium constant $k'_D = k'_a/k'_d$.

At the equilibrium of the recognition process, the relationship between the sensing signal and the analyte concentration can also be derived as

$$\delta I_{Analyte} \propto \delta\Gamma_{Analyte} = \frac{\frac{(\gamma_s)_0 \cdot c_{Ligand}}{K_D + c_{Ligand}} \cdot c_{Analyte}}{K'_D + c_{Analyte}} \cdot M_{Analyte} \approx \frac{(\gamma_s)_0 \cdot c_{Analyte}}{K'_D + c_{Analyte}} \cdot M_{Analyte} \tag{12}$$

As ligand concentration, c_{Ligand} , can be several magnitudes larger than K_D, making $\frac{K_D}{c_{Ligand}} + 1 \approx 1$, Obviously, Eqs. (11) and (12) have the same expression, indicating that the same formula can be used to fit both ligand immobilization and analyte binding.

4. Results and discussion

4.1. The linear relationship between the light reflection intensity and protein layer thickness

To verify the linear relationship between the light reflection intensity and protein layer thickness under the optimized conditions calculated in 3.1, the corresponding ellipsometry of the sensing signal, IE and SE are respectively used in this work. The measurement experiments of the ligand covalent immobilization and the analyte specific recognition are optimized by the incidence angle of 75° as well as the azimuths of $P = 90°$ and $A = 45°$, respectively. The surface modification of the amino silane self-assembly method is accomplished by coupling APTES with Glu-molecules, with the concentration and working conditions being adjusted in accordance with prior studies [19]. The results of surface sensing signal and layer thickness at various protein concentrations are presented in the Fig. 3. On the one hand, (a), (c) and (e) describe the change curves of the ligand surface sensing signals (black line) and the layer thickness (red line) of IgG, BSA and Fib with different concentrations. On the other hand, for the specific recognition of anti-igg, anti--BSA and anti-Fib, the curves of the sensing signal of IE and SE with the concentration of antibodies are shown in right column such as (b), (d), (f).

Furthermore, we have constructed the quantitative relationship curve between the thickness variation δd and the change of reflected light intensity δI of the various proteins bound to the same surface in Fig. 4. The linear regression analysis curve of the results showed that the correlation coefficient of the two variables is 0.993, within the confidence interval of 0.05, indicating a significant correlation. The slope, $k = 10.604 \pm 0.190$, illustrates the coefficient of the layer thickness and light intensity for the silicon substrate with a silica layer of

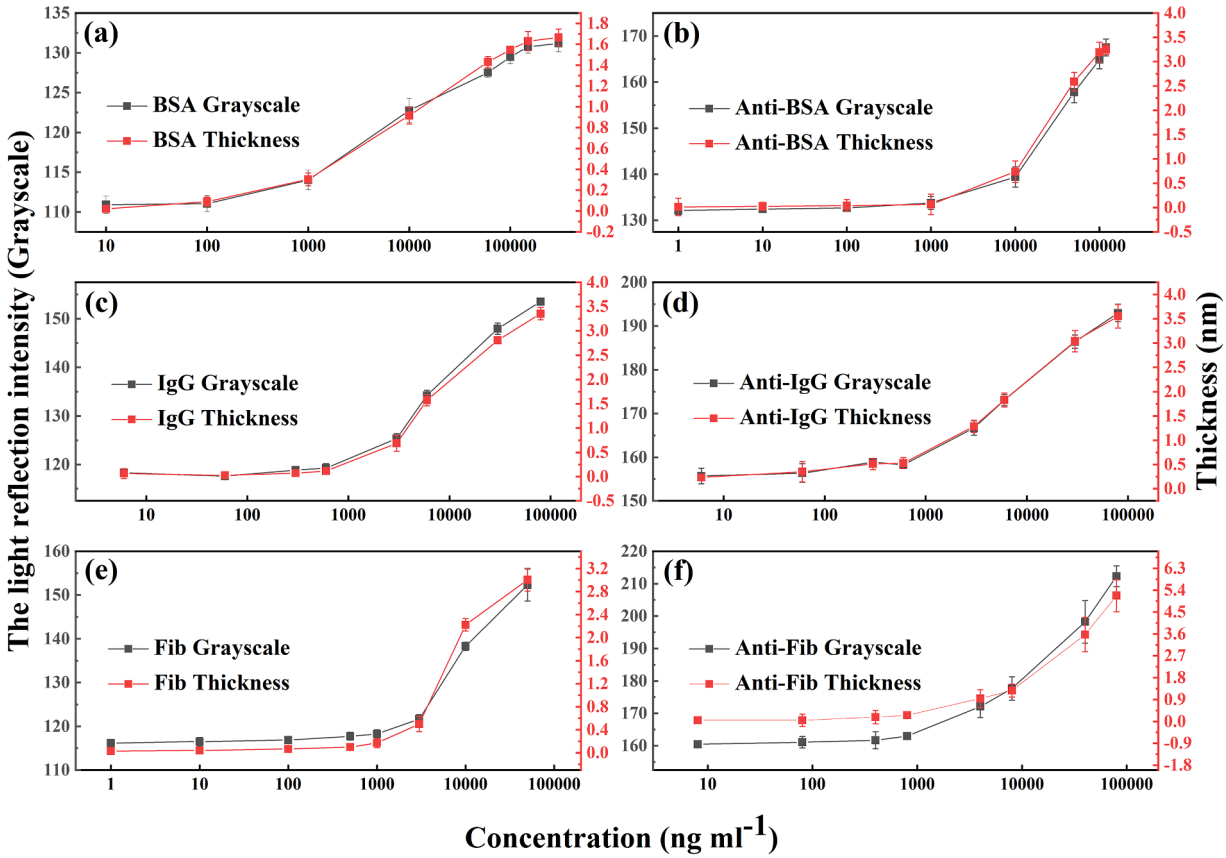

Fig. 3. The light reflection intensity (black line) and thickness (red line) corresponding to the binding surface of proteins at different concentrations.

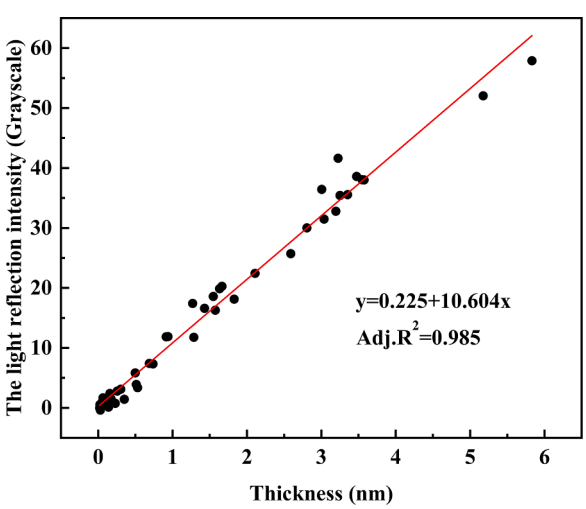

Fig. 4. The corresponding relationship of the variation between light reflection intensity and thickness for different analytes and ligands.

approximately 2 nm according to the Eq. (7), the relation is deduced as $\delta I = k{\cdot}\delta d$. The sensitive linear response of the sensing signal to the thickness is established at the optimal azimuth setting, which is consistent with the previous analysis.

4.2. The standard curve on the signal vs. sample concentration

Establishing a standard curve on the signal vs. sample concentration is the main goal of the BIE quantitative model. Fig. 5 depicts the change of the IE sensing signal for different concentrations of proteins, (a), (c) and (e) express the ligand binding of IgG, BSA and Fib proteins with different concentrations. On the other hand, for the specific recognition of anti-igg, anti-BSA and anti-Fib, the curves of the sensing signal of IE are shown in right column of Fig. 5 such as (b), (d), (f). Combined with the Eqs. (11) and (12), all the curves can be fitted to obtain the equilibrium dissociation rate constant shown in Table 1.

It became clear that in the process of ligand immobilization, Fib has the smallest dissociation constant and the strongest affinity with modified substrate, followed by IgG, and BSA has the weakest affinity due to its configuration which is difficult to expose the amino group. It is worth mentioning that all the dissociation equilibrium constants fitting of the binding processes are lower than 10^{-6} *M*, indicating that they are all strong interactions. The affinities of the specific protein binding processes are as anticipated, which confirm the quantitative model, and appropriate standard equations are derived, as shown in Fig. 4.

5. Conclusion

To bridge the gap between the biochemical demand and BIE, the signal response of BIE has been enhanced around 10 times in a linear off-null working condition optimized at the incidence angle of 75° with the fixed azimuths of the polarizer and the analyzer $P = 90°$ and $A = 45°$ Under the optimized working condition, the standard curves of ellipsometric signal vs. protein concentrations under three proteins are established by a quantitative model of binding process. The results would benefit the promotion and use of the sensor.

Declaration of Competing Interest

The authors declare that they have no known competing financial interests or personal relationships that could have appeared to influence the work reported in this paper.

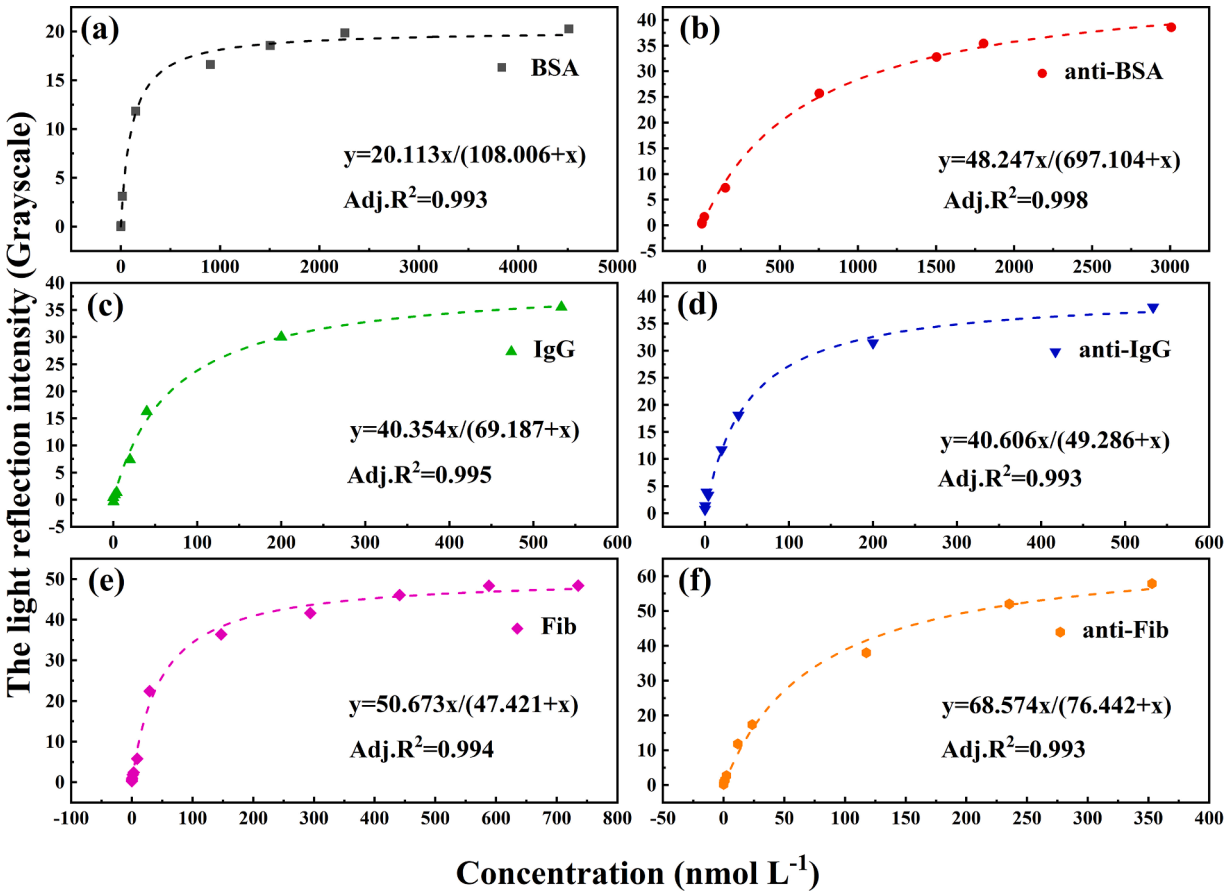

Fig. 5. The standard curves on the light reflection intensity vs. protein concentration.

Table 1
The equilibrium dissociation rate constant of various binding proteins.

ligand	$K_d(10^{-7}$ M)	Analyte	$K'_D(10^{-7}$ M)
BSA	10.801±1.704	Anti-BSA	69.709±6.790
IgG	6.919±0.787	Anti-IgG	4.929±0.604
Fib	4.742±0.586	Anti-Fib	7.644±1.185

[a]The error is an estimate of the coefficient of the curves in Fig. 5, satisfying a confidence interval of 0.05.

Data Availability

Data will be made available on request.

Acknowledgement

The authors thank the financial support to the National Natural Science Foundation of China (81872584).

References

[1] G. Jin, Y.H. Meng, L. Liu, Y. Niu, S. Chen, Q. Cai, T.J. Jiang, Development of biosensor based on imaging ellipsometry and biomedical applications, Thin Solid Films 519 (2011) 2750–2757, https://doi.org/10.1016/j.tsf.2010.12.175.
[2] Y. Niu, J. Zhuang, L. Liu, X. Yan, G. Jin, Two kinds of anti-ricin antibody and ricin interaction evaluated by biosensor based on imaging ellipsometry, Thin Solid Films 519 (2011) 2768–2771, https://doi.org/10.1016/j.tsf.2010.12.054.
[3] G. Jin, P. Tengvall, I. Lundstrom, H. Arwin, A Biosensor Concept Based on Imaging Ellipsometry for Visualization of Biomolecular Interactions, Anal. Biochem. 232 (1995) 69–72, https://doi.org/10.1006/abio.1995.9959.
[4] S.R. Urva, V.C. Yang, J.P. Balthasar, Development and Validation of an Enzyme Linked Immunosorbent Assay for the Quantification of Carcinoembryonic Antigen in Mouse Plasma, J. Immunoassay Immunochem. 30 (2009) 418–427, https://doi.org/10.1080/15321810903188227.
[5] Y.M. Bae, B.K. Oh, W. Lee, W.H. Lee, J.W. Choi, Detection of insulin-antibody binding on a solid surface using imaging ellipsometry, Biosens. Bioelectron. 20 (2004) 895–902, https://doi.org/10.1016/j.bios.2004.03.032.
[6] J. Hu, M.Y. Gao, Z.B. Wang, Y.J. Chen, Review on the applications of atomic force microscopy imaging in proteins, Micron (2022) 159, https://doi.org/10.1016/j.micron.2022.103293.
[7] S. Kurosawa, J.W. Park, H. Aizawa, S.I. Wakida, H. Tao, K. Ishihara, Quartz crystal microbalance immunosensors for environmental monitoring, Biosens. Bioelectron. 22 (2006) 473–481, https://doi.org/10.1016/j.bios.2006.06.030.
[8] C. Qi, J.Z. Duan, Z.H. Wang, Y.Y. Chen, P.H. Zhang, L. Zhan, X.Y. Yan, W.C. Cao, G. Jin, Investigation of interaction between two neutralizing monoclonal antibodies and SARS virus using biosensor based on imaging ellipsometry, Biomed. Microdevices 8 (2006) 247–253, https://doi.org/10.1007/s10544-006-8305-2.
[9] W. Wang, C. Qi, T.F. Kang, Y. Niu, G. Jin, Y.Q. Ge, Y. Chen, Analysis of the interaction between tropomyosin allergens and antibodies using a biosensor based on imaging ellipsometry, Anal. Chem. 85 (2013) 4446–4452, https://doi.org/10.1021/ac303783j.
[10] Y. Li, W. Liu, G. Jin, Y. Niu, Y. Chen, M. Xie, Label-Free Sandwich Imaging Ellipsometry Immunosensor for Serological Detection of Procalcitonin, Anal. Chem. 90 (2018) 8002–8010, https://doi.org/10.1021/acs.analchem.8b00888.
[11] Y. Niu, T.F. Kang, G. Jin, Joint detection of tumor markers with imaging ellipsometry biosensor, Thin Solid Films 571 (2014) 453–462, https://doi.org/10.1016/j.tsf.2014.01.043.
[12] M. Li, W. Liu, J.P. Correia, A.C. Mourato, A.S. Viana, G. Jin, Optical and Electrochemical Combination Sensor with Poly-Aniline Film Modified Gold Surface and Its Application for Dissolved Oxygen Detection, Electroanalysis 26 (2014) 374–381, https://doi.org/10.1002/elan.201300459.
[13] D.E. Aspnes, Spectroscopic ellipsometry - Past, present, and future, Thin Solid Films 571 (2014) 334–344, https://doi.org/10.1016/j.tsf.2014.03.056.
[14] H. Liu, J. Shen, W. Liu, Y. Niu, G. Jin, Imaging ellipsometry biosensor: basic theory, principles of operation, and applications, J. Vac. Sci. Technol. B. (2020) 38, https://doi.org/10.1116/1.5129596.
[15] H. Arwin, Optical-Properties of Thin-Layers of Bovine Serum-Albumin, Gamma-Globulin, and Hemoglobin, Appl. Spectrosc. 40 (1986) 313–318, https://doi.org/10.1366/0003702864509204.
[16] C.H. Huang, Q.L. Yang, F.Y. Song, N. Chen, X.L. Liao, B. Yao, S.T. Zhang, Y.Y. Chen, G. Jin, Site-directed immobilization antibody for alpha-fetoprotein detection by

optical biosensor, Integr. Ferroelectr. 171 (2016) 70–78, https://doi.org/10.1080/10584587.2016.1172004.

[17] H. Arwin, S. Welinklintstrom, R. Jansson, Off-Null Ellipsometry Revisited - Basic Considerations for Measuring Surface Concentrations at Solid Liquid Interfaces, J. Colloid Interface Sci. 156 (1993) 377–382, https://doi.org/10.1006/jcis.1993.1125.

[18] Y.Y. Chen, Y.H. Meng, G. Jin, Optimization of off-null ellipsometry for air/solid interfaces, Appl. Opt. 46 (2007) 8475–8481, https://doi.org/10.1364/Ao.46.008475.

[19] Z.H. Wang, Y.H. Meng, P.Q. Ying, C. Qi, G. Jin, A label-free protein microfluidic array for parallel immunoassays, Electrophoresis 27 (2006) 4078–4085, https://doi.org/10.1002/elps.200500956.